Computational Materials Science 230 (2023) 112502

Contents lists available at ScienceDirect

Computational Materials Science

journal homepage: www.elsevier.com/locate/commatsci

Full Length Article

Exploring the impact of backbone architecture on the thermal decomposition of silicon-containing arylacetylene resins

Yaxi Hu, Liquan Wang *, Liang Gao, Jiaping Lin *, Lei Du

Shanghai Key Laboratory of Advanced Polymeric Materials, Key Laboratory for Ultrafine Materials of Ministry of Education, Frontiers Science Center for Materiobiology and Dynamic Chemistry, School of Materials Science and Engineering, East China University of Science and Technology, Shanghai 200237, China

ARTICLE INFO

Keywords:
Thermal decomposition mechanisms
Silicon-containing arylacetylene resins
Reactive force field
Thermal stability

ABSTRACT

Silicon-containing arylacetylene (PSA) resins are promising heat-resistant polymers. However, little is known about their decomposition mechanisms. A molecular dynamics (MD) study based on reactive force field (ReaxFF) was employed to investigate the thermal decomposition mechanism of two representative PSA resins containing benzene or naphthalene in the backbone. The effect of heating rate, temperature, and crosslinking degree on decomposition behavior was examined, and the temperatures of three decomposition stages were disclosed. The predicted 5% decomposition temperatures (T_{d5}) and decomposition products are consistent with experimental findings. The ReaxFF MD simulation reveals that the T_{d5} is dominated by the secondary decomposition and final decomposition, in which the high molecular weight and the stable C—C bond of naphthyl play a dominant role in determining high-temperature resistance of the naphthalene-containing PSA resin. We also disclose the decomposition pathways of PSA-type resin. The results gained from the present work can be a helpful guideline for designing resins with excellent heat resistance.

1. Introduction

Silicon-containing arylacetylene (PSA) resins, a new type of organic–inorganic hybrid resin, have promising applications in aerospace and astronautics because of their excellent heat resistance [1–3]. The PSA with extremely high thermal stability was first exploited by Itoh et al. [4,5]. Afterward, diversified PSA resins emerged, some of which have a 5% decomposition temperature (T_{d5}) above 600 °C [6,7]. For example, Zhu et al. recently designed a new type of PSA resin through a materials genome approach. The new PSA resin, PSNP, contains naphthalene in the backbone. It exhibits a T_{d5} of 655 °C, bearing better heat resistance than traditional PSA resins [8,9]. Since the structure affects performance, conducting in-depth research on the pyrolysis mechanism at the atomic level is imperative to improve the heat resistance of PSA resins further.

Although there are many studies on the thermosetting mechanism of PSA resins, few reports on the degradation process, especially for the effect of backbone on PSA resins, are available. Zhang et al. conducted a study on PSA-type resins and found that SiO_2 and SiC appear on the surface of this resin during ablation, increasing the heat resistance [10]. They further explored the decomposition mechanism of an acetylene-functional benzoxazine-modified PSA-type resin (poly(dimethylsilyleneethynylene-phenyleneethynylene)). It was revealed that introducing alkynyl groups can enhance the activity of the *para*-position of the aniline ring due to the emergence of 3,4-dimethylaniline. Therefore, avoiding more alkynyl groups is conducive to improving heat resistance [7]. Guo et al. explored the thermal degradation behavior of PSAs with various pendant groups [11]. Although PSAs with various substituents have different kinds of pyrolysis products and pyrolysis temperatures, thermogravimetric-gas chromatography-mass spectrometry (TG-GC–MS) characterization revealed a general rule, i.e., the Si-CH_3 and other aliphatic structures first fall off from the main chain and turn into CH_4, followed by the formation of C_2H_4 and C_2H_6, H_2 is released at last as the temperature rises.

Experimental characterization methods such as thermogravimetric analysis (TGA) were commonly applied to explore the thermal properties [12]. However, the detailed decomposition mechanism of PSA resins with different backbones remains unclear due to the limitation of methods in characterizing the complex evolution of free-radical fragments. In recent years, quantum chemistry (QC) methods have achieved high prediction accuracy and provided helpful theoretical guidance, but calculation scales are limited due to the high computational costs

* Corresponding authors.
E-mail addresses: lq_wang@ecust.edu.cn (L. Wang), jlin@ecust.edu.cn (J. Lin).

https://doi.org/10.1016/j.commatsci.2023.112502
Received 29 May 2023; Received in revised form 6 September 2023; Accepted 8 September 2023
Available online 18 September 2023

[13–15]. On the other hand, classical molecular dynamic (MD) simulations only considered the interactions between the nucleus, rendering it unsuitable for describing chemical reactions [16,17]. Recently, reactive force field (ReaxFF), a combination of QC and MD methods, has emerged as a feasible method to solve the above problems and reveal the degradation mechanism of polymers [18,19]. The ReaxFF makes MD simulation in complicated reactive chemical systems practical by combining bond-order functions and polarizable charge descriptions.

The ReaxFF has developed rapidly since it was put forward, and now it plays a vital role in predicting the decomposition mechanism of polymers [20–22]. For example, Lu et al. conducted a ReaxFF MD simulation to study the pyrolysis process of polyimide and explored the formation mechanism of decomposition products [23]. Through ReaxFF MD simulations, Zhong et al. studied the decomposition pathway of phenolic resin and proposed two possible thermal decomposition paths of phenolic hydroxyl groups [24]. They also suggested a theoretical basis for improving the heat resistance of resins. The ReaxFF CHON-2019 developed by Kowalic et al. was employed to investigate the blends of polyacrylonitrile and poly(*p*-phenylene-2,6-benzobisoxazole) in the work of Mao et al. [25]. They found that O-containing groups effectively participate in the initial reaction, while N-containing groups are essential in forming graphite networks [26]. As for the PSA-type resins, an in-depth understanding of the thermal decomposition mechanism can help design resins with high thermal stability. However, little is known about the effect of the backbone structure on the decomposition mechanism [11,27–30].

In the present work, we chose two crucial kinds of PSA resins to gain insight into the degradation mechanisms. One is the PSNP resin containing 2,7-diethynylnaphthalene in the backbone designed by Zhu et al., and the other is the classical PSA-Phen resin containing benzene in the backbone [8]. ReaxFF MD simulation was conducted to track the products and bonds in the decomposition of PSA resins. First, the effects of heating rate, temperature, and crosslinking degree on the degradation of PSNP and PSA-Phen resins were examined from the atomic level. Then, we analyzed first-order kinetics to understand the kinetic behaviors of the decomposition of resins. Furthermore, the simulation results were compared with experiments, and a good agreement was found. Finally, the possible reaction pathways were proposed to understand the pyrolysis process deeply. This work reveals the thermal decomposition mechanism of PSA resins that is difficult to be obtained by experiments from the atomic scale and explains why the newly designed PSNP resins had better heat resistance than PSA-Phen resins.

2. Computational methodology

We considered bulk systems containing PSA-Phen or PSNP resins. The repeat units of these two resins are shown in Fig. 1(a). PSA-Phen resins, bearing high thermal stability, are the classical resins developed by Itoh et al. [4,5]. PSNP resins are a new kind of heat-resistant PSA resins recently designed by the materials genome approach [8]. The thermal properties of these two resins are summarized in Table 1.

We first placed chains with three repeating units into a simulation box to more precisely meet pre-polymerization conditions in experiments [8,31]. Then, a crosslinking procedure was adopted to form three-dimensional network structures. During the curing process of PSA-type resins, the alkynyl group can undergo Diels-Alder reaction, cyclotrimerization, and free radical polymerization reaction to form various crosslinked structures, such as naphthalene ring, benzene ring, and polyene [32,33]. Since the Diels-Alder cycloaddition plays a dominant role in the curing process [10,34,35], we only considered the Diels-Alder cycloaddition during crosslinking in the present work. Fig. 1(b) depicts the Diels-Alder reaction of PSA-Phen and PSNP resins. In the crosslinking procedure, thirty prepolymer chains were included in the simulation box, and the crosslinking degrees of 10%, 40%, 70%, and 100% were adopted to explore the relationship between the crosslinking degree and pyrolysis (for details about the crosslinking procedure, see Section 1 of the Supporting Information). The modeling and crosslinking procedures were implemented in MD simulation with Materials Studio [36].

After crosslinking, the remaining MD simulation was performed by the "user-reaxc" package in LAMMPS [37]. The ReaxFF parameters applied in this work are composed of C, H, and Si elements, previously parameterized by Kulkarni et al.[38] In ReaxFF, the energy E_{system} of the system is given as

$$E_{system} = E_{bond} + E_{over} + E_{angle} + E_{tors} + E_{vdWaals} + E_{Coulomb} + E_{Specific} \quad (1)$$

where E_{bond}, E_{over}, E_{angle}, E_{tors}, $E_{vdWaals}$,$E_{Coulomb}$ and $E_{Specific}$ represent bond energy, over-coordination penalty energy, angle strain energy, torsional angle energy, van der Waals energy, Coulomb energy, and some other specific terms that are not generally included unless required, such as long-pair electron energy and conjugation energy [15,39].

ReaxFF judges the connection between atoms through the bond order (BO'_{ij}), thus simulating the breaking and forming of bonds and evaluating the decomposition products. The atomic charge was continuously updated as the changes in atomic distance, and the r_{ij} at the next moment was calculated to obtain a new BO'_{ij}. The BO'_{ij} is calculated as

Table 1
Thermal properties of the PSA-Phen and PSNP resins.

Resins	PSA-Phen	PSNP
T_{d5} (°C)	627	655
$Y_{800\ °C}$ (%) *	90.3	92.3
*$Y_{800\ °C}$: Residual yield at 800 °C		

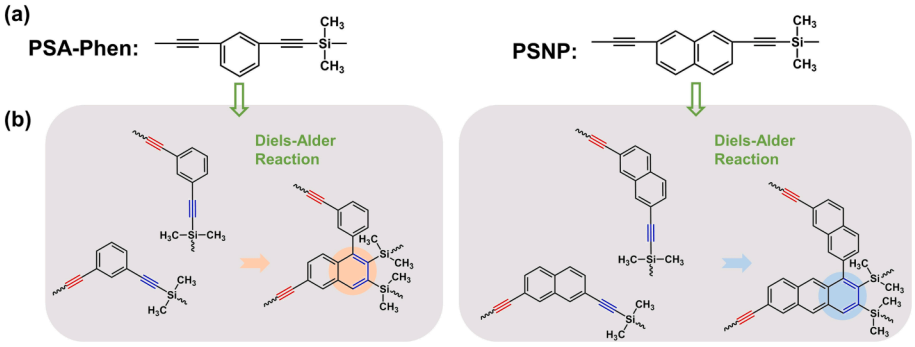

Fig. 1. (a) Repeat units and (b) Diels-Alder reaction during the curing process of PSA-Phen and PSNP resins. The Diels-Alder cycloaddition is the crosslinking reaction of alkyne units considered in the MD simulation. The cured structures of PSA-Phen and PSNP resins formed by the Diels-Alder reaction are marked with orange and blue regions, respectively. (For interpretation of the references to colour in this figure legend, the reader is referred to the web version of this article.)

$$BO'_{ij} = BO^{\sigma}_{ij} + BO^{\pi}_{ij} + BO^{\pi\pi}_{ij} = \exp\left[p_{\mathrm{bo1}}\left(\frac{r_{ij}}{r^{\sigma}_{\mathrm{o}}}\right)^{p_{\mathrm{bo2}}}\right] + \exp\left[p_{\mathrm{bo3}}\left(\frac{r_{ij}}{r^{\pi}_{\mathrm{o}}}\right)^{p_{\mathrm{bo4}}}\right] + \exp\left[p_{\mathrm{bo5}}\left(\frac{r_{ij}}{r^{\pi\pi}_{\mathrm{o}}}\right)^{p_{\mathrm{bo6}}}\right] \quad (2)$$

where r_{o} terms are equilibrium bond lengths, and p_{bo} terms are empirical parameters. BO^{σ}_{ij}, BO^{π}_{ij}, $BO^{\pi\pi}_{ij}$ represent a single bond, double bond, and triple bond, respectively.

In this work, we used$BO'_{ij} = 0.3$ as the criterion for judging whether the chemical bond breaks or not [25,40]. As$BO'_{ij} \geq 0.3$, the chemical bond is considered to be formed. Otherwise, the chemical bond is considered to be broken. Using this criterion, we readily analyzed the decomposition products in terms of the bond order and the trajectory file.

In the ReaxFF MD simulation, the cured systems were first equilibrated at 300 K in an *NPT* ensemble for 50 ps to eliminate internal stress. And then, an annealing procedure was performed five times between 300 K and 600 K in the *NVT* ensemble to produce more reasonable structures, which lasted 25 ps. Subsequently, a cook-off process was performed, where the temperature was heated from 300 K to a targeted temperature in the range of 1400–3000 K with an interval of 100 K at varied heating rates (50 K/ps, 100 K/ps, 200 K/ps, and 500 K/ps). Finally, a 300 ps pyrolysis process was carried out in the *NVT* ensemble. The temperature in the present simulations was controlled by a Berendsen thermostat with a damping constant of 50 fs [41]. The time step is 0.1 fs.

3. Results and discussion

Dividing the decomposition process of PSA-type resins into several stages according to the shedding and generation evolution tendency of fragments is beneficial for analyzing their thermal decomposition mechanisms [42]. Therefore, the thermal decomposition process is divided into three stages, i.e., initial, secondary, and final decompositions, in this work. In the stage of initial decomposition, bonds in the cured resins break, and free radicals appear. In the secondary reaction, the radicals attack other radicals or molecules to form new structures. At last, in the final decomposition, the various newly formed structures decompose again, and the number of radicals increases. Subsequent analyses are based on the above three stages.

3.1. Effect of heating rate on the degradation process of PSA-type resins

The effect of the heating rate on the number of degradation products and bonds was examined. We considered the crosslinking structures of the PSA-Phen and PSNP resin with a crosslinking degree of 70%. The temperature was increased from 300 to 3000 K at heating rates of 50, 100, 200, and 500 K/ps. The whole process lasted for 80 ps.

The dominant decomposition products include methane, acetylene, hydrogen, and some benzene/naphthalene-containing structures. The temporal evolution of the dominant fragments at various heating rates is shown in Fig. 2. CH_4 and benzene/naphthalene-containing structures are primary and secondary decomposition products. C_2H_2 and H_2 are the products of the secondary and final reactions. The amount of CH_4 and benzene/naphthalene-containing structures decreases gradually after reaching the peak of fragments number. The CH_4 forms earlier than benzene/naphthalene-containing structures, but the peak of the CH_4 number appears later. Neither C_2H_2 nor H_2 appears at the heating rate of 50 K/ps in PSA-Phen resins, but they appear in the decomposition process of PSNP resins. The C_2H_2 nor H_2 appear earlier under higher heating rates.

As shown in Fig. 2, the temperatures at which PSA-Phen resin begins to decompose are ca. 1719.3, 2191.7, 2355.1, and 2862.2 K, and the initial decomposition temperatures for PSNP resin are about 2054.1, 2266.0, 2497.8, and 2989.3 K for the heating rates of 50, 100, 200, and 500 K/ps, respectively. In addition, the times at which PSA-Phen resin begins to decompose are ca. 28.5, 18.9, 10.5, and 5.4 ps, and the initial decomposition times for PSNP resin are about 35.3, 19.9, 11.2, and 5.5 ps for the heating rates of 50, 100, 200, and 500 K/ps, respectively. This indicates that with increasing heating rates, the initial decomposition temperature increases, and the initial decomposition time decreases, which is in good agreement with the experiments [30].

In this work, we approximately defined the time at which the number of benzene/naphthalene-containing structures begins to decrease as the

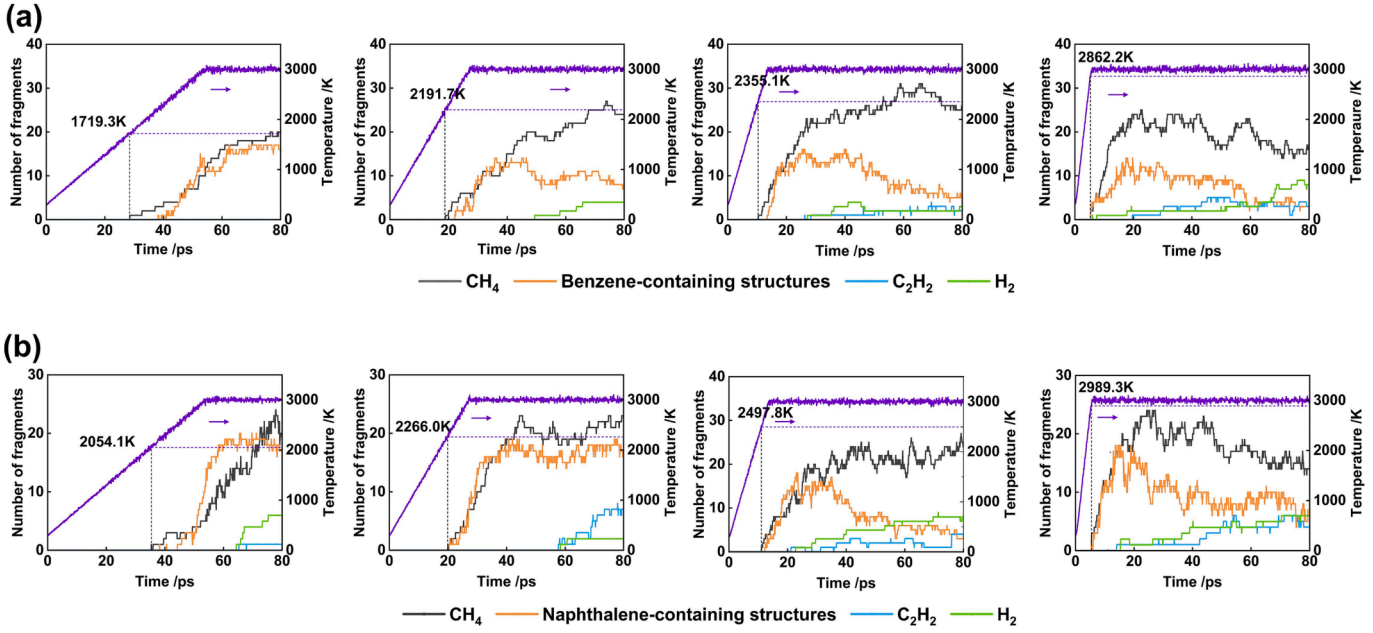

Fig. 2. Temporal evolution of the dominant fragments for the decomposition of (a) PSA-Phen and (b) PSNP resins heated from 300 to 3000 K at the heating rates of 50, 100, 200, and 500 K/ps. The black, blue, and green lines correspond to CH_4, C_2H_2, and H_2, respectively. The orange lines represent benzene-containing structures in PSA-Phen resins and naphthalene-containing structures in PSNP resins. The purple lines represent the temperature change in the simulation. (For interpretation of the references to colour in this figure legend, the reader is referred to the web version of this article.)

secondary decomposition time and the time at which the number of benzene/naphthalene-containing structures starts to be constant as the final decomposition time. From Fig. 2, we can learn that both the secondary and final decomposition times decrease as the heating rate increases. Moreover, secondary decomposition was found to occur after reaching the targeted temperature.

We also investigated the evolution of bonds and molecules under various heating rates (see section 2 of the Supporting Information). Compared with the PSA-Phen resin, the PSNP resin produced more C—C bonds, fewer C—H bonds, and almost the same number of C-Si bonds during decomposition at the same heating rates. Although PSNP resin has more unsaturated bonds than PSA-Phen resin before decomposition, the total number of bonds increased in the decomposition of PSNP resin is less, indicating that PSNP resin has better heat resistance than PSA-Phen resin.

3.2. Effect of temperature on the degradation process of PSA-type resins

The same crosslinking models as in section 3.1 were used to study the influence of temperature. To investigate the effect of different targeted temperatures and minimize the effect of heating rates on decomposition, we adopted 500 K/ps as the heating rate from 300 K to a targeted temperature during the ramp. A high heating rate like 500 K/ps is beneficial to preserve an intact resin structure when the targeted decomposition temperature is reached. After achieving the targeted temperature, a 300 ps simulation of the pyrolysis process, in which significant information for decomposition can be gained, was carried out to examine the effect of temperature on the degradation process. The targeted temperature ranges from 1400 K to 3000 K.

Fig. 3 shows the number of primary products produced by decomposing PSA-Phen and PSNP resins at a targeted temperature between 1400 K and 3000 K. The tendency of product variation with temperatures for PSA-Phen resins is similar to that for PSNP resins. CH_4 is the majority product of the decomposition, followed by benzene/naphthalene-containing structures, C_2H_2, H_2, C_2H_4, and C_2H_6. The number of C_2H_2 and H_2 keeps rising with increasing temperature. In contrast, the number of other products first increases and then decreases as the temperature increases, where the maximum appears between 2000 K and 2400 K, which indicates that the influence of secondary decomposition dominates in the range from 2000 K to 2400 K.

We noted that the number of benzene and naphthalene-containing structures decreases as the temperature exceeds ca. 2100 K. The generation of benzene and naphthalene-containing structures from the pyrolysis of resins and the thermal decomposition of benzene/naphthalene rings occur at high temperatures. The two effects should be more evident as the temperature increases. As the decomposition of benzene/naphthalene rings dominates over the generation of benzene and naphthalene-containing structures from resin pyrolysis, the apparent number of benzene and naphthalene-containing structures decreases. This is a competition between the generation of benzene and naphthalene-containing structures from resin pyrolysis and the decomposition of benzene/naphthalene rings.

Fig. 4 shows the number of bonds for these products from the decomposition with increasing temperatures. Due to the absence of the concept of the bond in ReaxFF simulations, "-" was used to represent the connections between two atoms (including single, double, and triple bonds). For example, C—C includes carbon–carbon single bonds, double bonds, and triple bonds. Therefore, we counted all types of C—C bonds (C—C, C═C, C≡C) as C—C connections. As can be seen, the number of C—C bonds increases to the highest value at 2600 K and then decreases rapidly.

When the temperature is lower than 2600 K, a large number of carbon-containing free radicals are generated. As the decomposition proceeds, more and more radicals are produced, attacking the uncrosslinked C≡C to form double or single bonds. When the temperature is higher than 2600 K, from the perspective of C—C, the structures

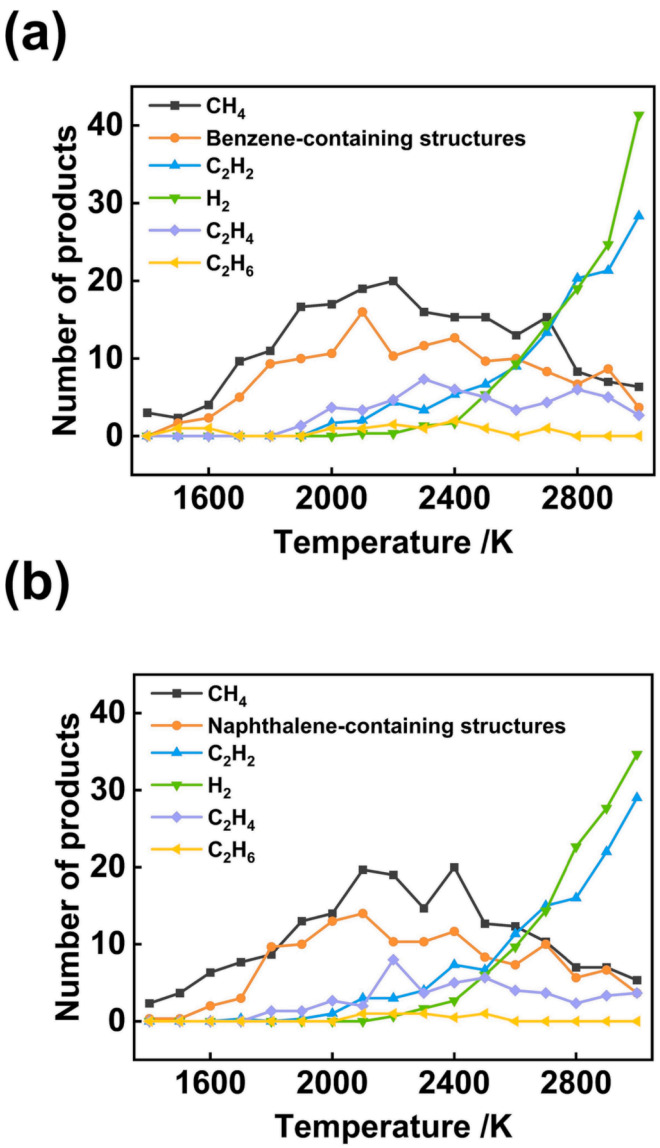

Fig. 3. The number of products decomposed from (a) PSA-Phen and (b) PSNP resins. Lines with various colors denote different products. The black, blue, green, purple, and yellow lines represent CH_4, C_2H_2, H_2, C_2H_4, and C_2H_6, respectively. The orange lines represent benzene-containing structures in the PSA-Phen resins, while they denote naphthalene-containing structures in the PSNP resins. (For interpretation of the references to colour in this figure legend, the reader is referred to the web version of this article.)

produced in the secondary reaction are broken again and become free radicals. As for C—H bonds, the number decreases with temperature rises, implying that the breaking rate of C—H is faster than its formation rate. It can be seen from Fig. 4(c) that under the same degree of crosslinking, the decomposition trends of the C-Si bond of PSA-Phen resin and PSNP resin are almost the same, suggesting that the introduction of benzene or naphthalene rings in the backbone of PSA-type resins has a less marked effect on the bond energy of C—Si bonds. To prove this, we calculated the bond dissociation energy (BDE) of C-Si bonds in the cured PSA-Phen and PSNP resins (for the structures used for calculation and results, see Section 3 of the Supporting Information). The results show that the BDE of the C-Si bonds in PSA-Phen and PSNP resins are almost similar. This can be the reason that the backbone morphology has a less pronounced influence on the thermal decomposition of C-Si bonds.

Shown in Fig. 5 is a plot of the number of molecules and bonds from decomposition against temperature. As can be seen, with increasing

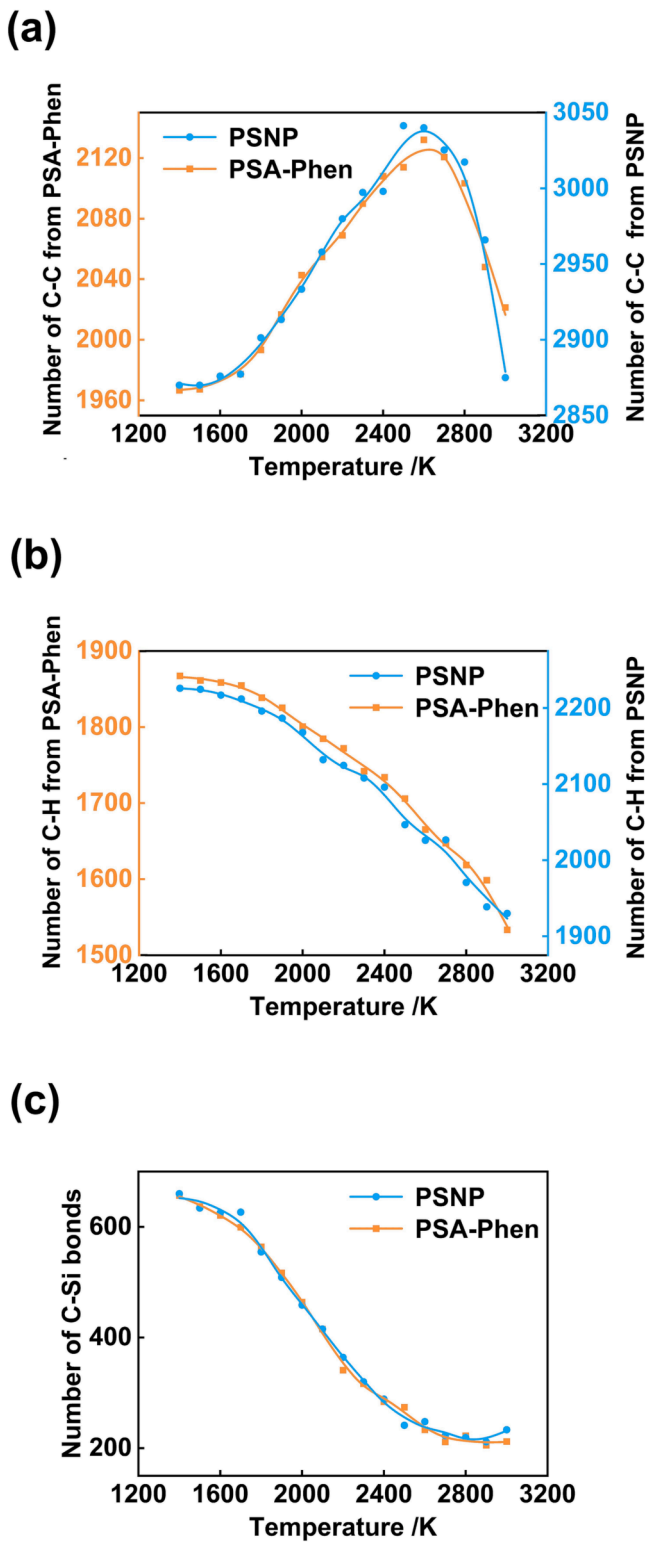

Fig. 4. Time evolution of the number of (a) C—C, (b) C—H, and (c) C—Si bonds in the decomposition products of the PSA-Phen and PSNP resins with temperatures ranging from 1400 to 3000 K. The orange lines represent the PSA-Phen resins, and the blue lines represent the PSNP resins. (For interpretation of the references to colour in this figure legend, the reader is referred to the web version of this article.)

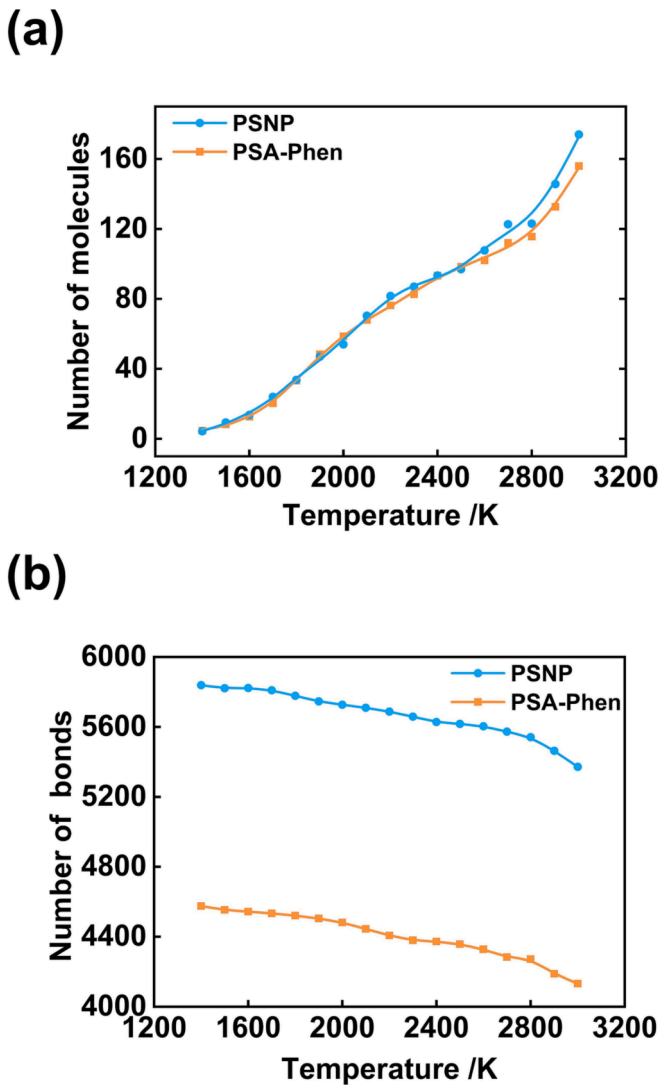

Fig. 5. The number of (a) total molecules and (b) total bonds in the decomposition products of the cured PSA-Phen and PSNP resins with the temperature ranging from 1400 to 3000 K. The orange lines and blue lines represent the PSA-Phen and PSNP resins, respectively. (For interpretation of the references to colour in this figure legend, the reader is referred to the web version of this article.)

temperature from 1400 to 3000 K, the number of molecules rises, but the number of bonds decreases. In terms of molecules, the PSA-Phen and PSNP resins have approximately the same number of molecules at a lower temperature, indicating that the initial decomposition rate of these two resins is almost the same due to their structures being close to each other. However, when the temperature exceeds 2600 K, the molecules from the PSNP resin are more than those from the PSA-Phen resin. This means that the decomposition of benzene, naphthalene, and anthracene is dominant at a temperature higher than 2600 K. The products of the PSNP resin are more than the PSA-Phen resin since it has more complicated structures (naphthalene and anthracene for the cured PSNP resin, while benzene and naphthalene for the cured PSA-Phen resin). In terms of bonds, the decreasing tendency of the two resins is similar, and the breaking rate of bonds increases as the temperature rises. Both the variation rates of the total number of molecules and bonds change significantly after 2600 K. This is due to the products reaching the peak value at 2000–2400 K and beginning to decompose again, and the final decomposition dominants after 2600 K, which leads to a significant change in the total number of molecules and bonds. From

the results mentioned above, we learned that the initial decomposition is dominant below 2000 K, the secondary decomposition plays a leading role in the range from 2000 K to 2400 K, and 2600 K is the boundary between the secondary and final decomposition.

3.3. Effect of crosslinking degree on the degradation process of PSA-type resins

The degree of crosslinking plays a vital role in the heat resistance of thermosetting resins [43,44]. To evaluate the relationship between crosslinking degree and T_{d5} of PSA-type resins, we examined the temporal evolution of main pyrolysis fragments of PSA-Phen and PSNP resins with the crosslinking degrees of 10%, 40%, 70%, and 100%. The temperature was quickly raised to 2600 K at a heating rate of 500 K/ps, and the decomposition was carried out for 300 ps.

As shown in Fig. 6, the products are mainly CH_4, benzene- and naphthalene-containing structures, C_2H_2, and H_2 for various crosslinking degrees. When the decomposition is performed at a high temperature of 2600 K, the initial and secondary decompositions take place in a short period. Fig. 6 shows that the number of CH_4 and benzene- or naphthalene-containing structures increases rapidly and then enters the final decomposition, where the numbers drop. The C_2H_2 and H_2, as the products of secondary decomposition and final decomposition, continue to increase in quantity.

The curves of CH_4 and C_2H_2 hardly change with the change of crosslinking degree, indicating that the crosslinking degree has a less marked effect on the amount of them. The peak of the number of fragments containing benzene and naphthalene reaches a maximum and tends to decrease with the increase of the degree of crosslinking. It indicates that the number of benzene- and naphthalene-containing structures decreases as the degree of crosslinking increases. When the resins are entirely crosslinked by the Diels-Alder reaction, the benzene- and naphthalene-containing structures become less, and none of their fragments is detected during the whole 300 ps decomposition process at 2600 K. This suggests that the increase of crosslinking degree is beneficial to reduce the decomposition products of PSA-type resins.

We then counted the number of C—C, C—H, and C-Si bonds in the decomposition process every 50 ps, where the obtained results are shown in Fig. 7. As can be seen in Fig. 7a, during the decomposition process, the triple and double bonds gradually break into single bonds, increasing the number of C—C bonds. It is also noted that the increase of crosslinking degree leads to an increase in the number of C—C bonds due to the Diels-Alder cycloaddition reaction, resulting in a higher number of C—C bonds in PSNP resin than in PSA-Phen. The number of C—H bonds shows a downward shift and decreases as crosslinking degrees increase (see Fig. 7b). The number of C—Si bonds decreased first and then reached a plateau as the thermal decomposition proceeded (Fig. 7c). The dissociation rate of C—Si bonds for different crosslinking degrees is almost the same at the beginning of decomposition.

However, for a long decomposition time, the number of C—Si bonds for the resins with higher crosslinking degrees is higher than those with lower crosslinking degrees. The Diels-Alder cycloaddition does not alter the C—Si bonds. However, it creates adjacent C-Si bonds on the benzene ring (see Fig. 1), which can increase the probability of forming new C—Si bonds between decomposed Si/C radicals and the surrounding C/Si atoms. Therefore, the number of C—Si bonds increases as the crosslinking degree increases.

From the exploration of the influence of crosslinking degree on thermal decomposition, we get to know that the higher crosslinking degree causes fewer decomposition products, leading to the enhanced heat resistance of the PSA-type resin. The changes in the number of total molecules and total bonds throughout the simulation were also examined to verify the results (see Section 4 of the Supporting Information).

3.4. Kinetic analysis of the degradation process of PSA-type resins

It is vital to obtain first-order kinetic information on pyrolysis by examining the consumption rate of reactants [45,46]. To get insight into the kinetic properties of PSA-Phen and PSNP resin degradation, we examined first-order kinetics to reveal the kinetic mechanisms of the resin degradation. Arrhenius plot of reaction rate constant k is generated according to the Arrhenius formula

$$\ln k = \ln A - E_a/RT \tag{2}$$

where A, E_a, R, and T denote the pre-exponential factor, activation energy, molar gas constant, and temperature, respectively. And the reaction rate constant k is determined by

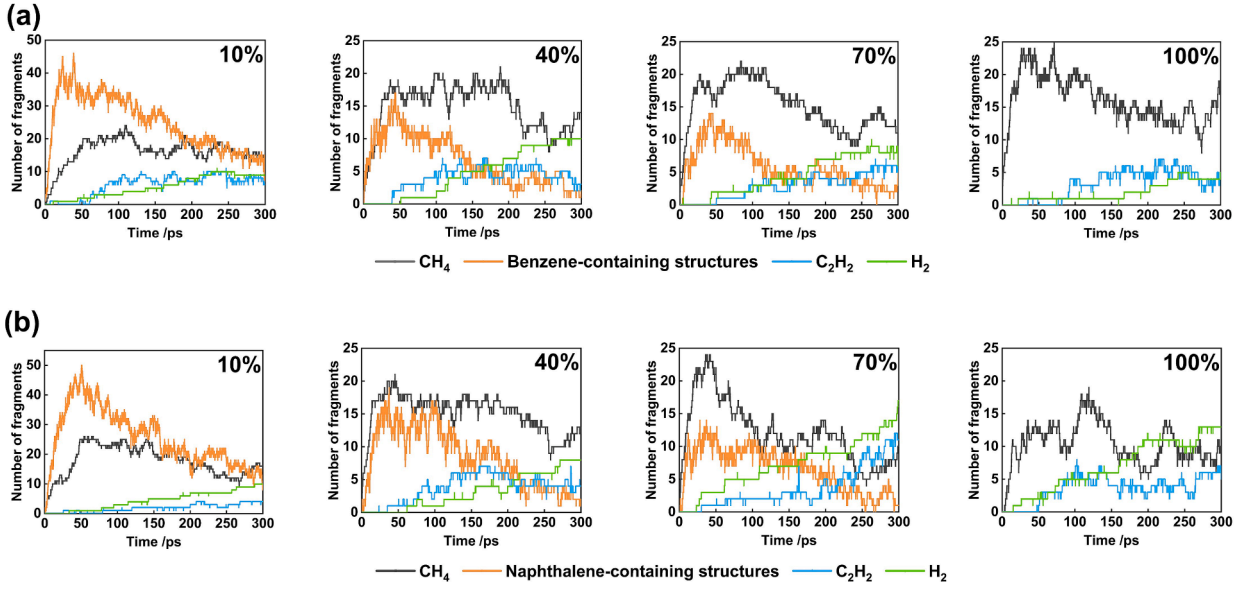

Fig. 6. The evolution of the main fragments from the decomposition of (a) PSA-Phen, and (b) PSNP with the crosslinking degree of 10%, 40%, 70%, and 100% at 2600 K with the heating rate of 500 K/ps. The black, blue, and green lines represent CH_4, C_2H_2, and H_2, respectively. The orange lines represent benzene-containing structures in the PSA-Phen resins, while they denote naphthalene-containing structures in the PSNP resins. (For interpretation of the references to colour in this figure legend, the reader is referred to the web version of this article.)

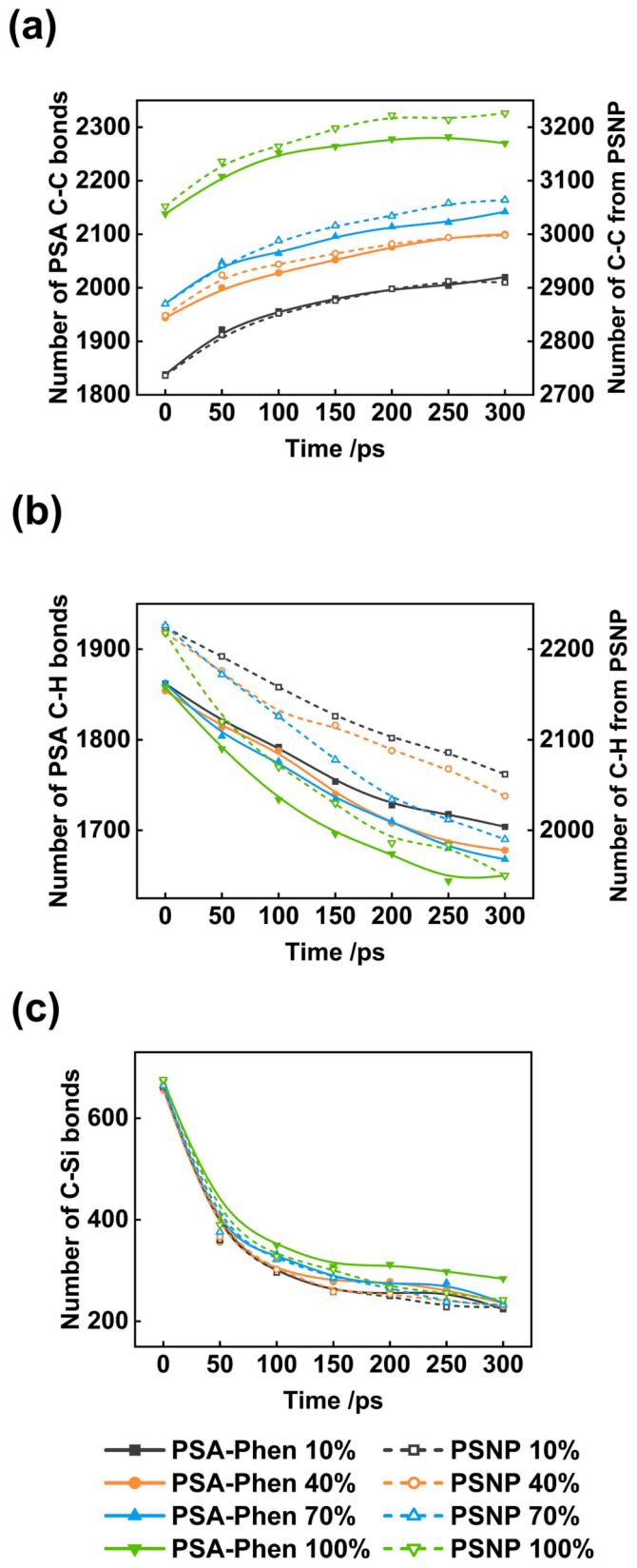

Fig. 7. Temporal evolution of the number of (a) C—C, (b) C—H, and (c) C—Si bonds in the decomposition products of PSA-Phen and PSNP systems with various crosslinking degrees at 2600 K. The black, orange, blue, and green lines represent the crosslinking degree of 10%, 40%, 70%, and 100%, respectively. The solid lines denote PSA-Phen resins, and the dashed lines denote PSNP resins. (For interpretation of the references to colour in this figure legend, the reader is referred to the web version of this article.)

$$\ln N_0 - \ln N_t = kt \tag{3}$$

where N_0 and N_t represent the number of resin molecules initially and at the degradation time t.

The activation energies of the degradation of PSA-type resins are essential for understanding the mechanism of thermal decomposition and polymer design. To count the number of molecules in the reconstituted or undecomposed resins, 30 prepolymers of the PSA-Phen and PSNP with three repeat units were decomposed under the temperature of 1600–2600 K for 10 ps. Three replicate simulations in the activation energy of PSA-Phen and PSNP resins were run, and the corresponding Arrhenius plot is shown in Fig. 8. The fitting parameters are listed in Table 2. It can be seen that the numerical value of the slope in Fig. 8 is similar to each other, and the activation energy of the degradation of PSA-Phen and PSNP resin is 139.30 kJ/mol and 156.53 kJ/mol, respectively. In the experiment performed by Xu et al., the activation energy of the decomposed PSA-Phen resin is determined as 149 kJ/mol by the Kissinger method and 153 kJ/mol by the Flynn-Wall-Ozawa method [47], which is close to the ReaxFF MD simulation results. These results well validated our simulation data. It is noteworthy that the activation energy of PSNP is slightly higher than that of PSA-Phen in simulation. The higher activation energy leads to fewer molecules with enough energy to overcome the potential barrier at a certain temperature, which verifies the experimental results of a higher 5% decomposition temperature of PSNP resin [8].

3.5. Comparison with experiments and decomposition mechanism

To validate ReaxFF results, we compared the simulation results with the reported experimental findings [8,11]. The comparison results are shown in Fig. 9. The difference in two TGA curves (orange and green) for the PSA-Phen system probably come from the difference in the sample purity, instruments, and operations. Such a difference can be acceptable because the two TGA curves were replotted from the reports of two research groups. The experiment represented by the orange line was performed by Zhu et al. [8], and the experiment represented by the green line was completed by Guo et al. [11]. We also conducted ReaxFF simulations for these systems. In the ReaxFF simulation, the PSA-Phen and PSNP resins were decomposed in a temperature ranging from 600

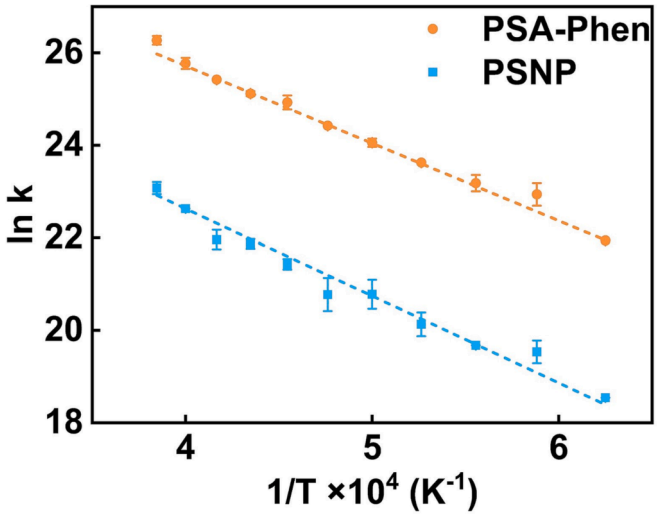

Fig. 8. Arrhenius plots of the rate constants (k) in the decomposition of PSA-Phen and PSNP resins. Orange represents PSA-Phen resins, while blue represents PSNP resins. Each point in the graph represents the average value of three replicate simulations, and the error bars represent their standard deviations. The dashed lines are fitted by these data. (For interpretation of the references to colour in this figure legend, the reader is referred to the web version of this article.)

Table 2
Fitting Arrhenius parameters of PSA-Phen and PSNP resins.

Resins	Temperature conditions	E_a (kJ/mol)	A (1/s)
PSA-Phen	1600–2600 K	139.30	1.20×10^{14}
PSNP	1600–2600 K	156.53	1.25×10^{13}

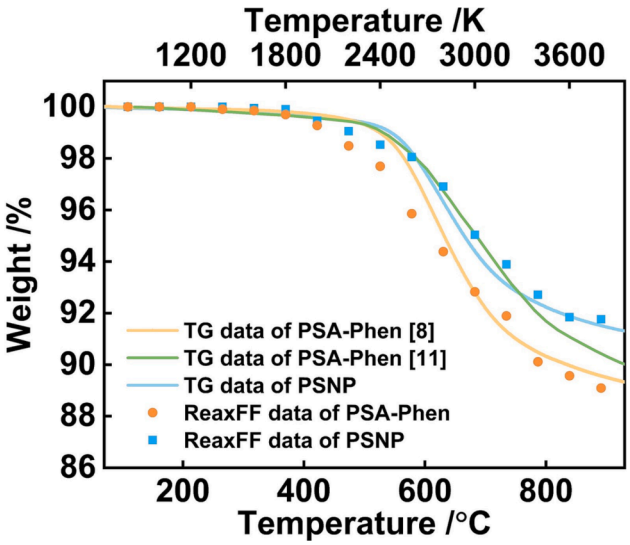

Fig. 9. Comparison of TGA curves with simulation results of PSA-Phen and PSNP resins. The points are the simulation data, and TGA curves are reproduced from the experiments in the literature (10 °C /min in N_2). The orange and blue line is reproduced from Ref 8 with permission. Copyright 2020 American Chemical Society. The green line is reproduced from Ref 11 with permission. Copyright 2016 Elsevier. (For interpretation of the references to colour in this figure legend, the reader is referred to the web version of this article.)

to 3800 K, with an interval of 200 K and a heating rate of 500 K/ps for 5 ps. One can see that the results of the ReaxFF simulation are relatively close to the two experimental results and can capture the feature that the PSNP resin is more thermally stable than the PSA-Phen.

Furthermore, it can be seen that the temperature range for T_{d5} of these resins is 2400–3000 K, and in this temperature range, the decomposition process is dominated by the secondary or final decomposition. In the secondary and final decomposition, the methyl groups, benzene/naphthalene-containing groups dropped in the initial decomposition, recombined with other radicals to form new structures, and decomposed again. During the final decomposition, the activation energy of the C—C bond breaking in naphthalene is higher than that of benzene (for the detailed calculation results, see Section 5 of the Supporting Information) [48], and the molecular weight of naphthalene is larger than that of benzene, therefore, PSNP resin has higher thermal stability. The above results indicate that introducing the naphthalene ring into PSA-type resins plays a decisive role in increasing the T_{d5} of PSNP resins. Furthermore, we fitted the simulation points to get the predicted residual yield at 800 °C ($Y_{800\ °C}$). The results are listed in Table 3. It can be seen that the simulation results are consistent with the experiments, which also verifies the accuracy of our ReaxFF MD simulations.

The decomposition mechanism of these resins was further analyzed by ReaxFF MD simulations at 2200 K. Through the mechanism analysis based on ReaxFF MD, the detailed thermal decomposition processes that cannot be obtained experimentally were revealed. The primary decomposition pathway and products were tracked and depicted in Fig. 10. In the simulation, the PSA-type resins were decomposed to generate various reactive groups in the initial stage. It can be seen that the pendant group (CH_3) of both PSA-Phen and PSNP resins first falls off at the beginning of decomposition, followed by H and SiC_2H_6, which means the pendant groups are in the weakest position in thermal decomposition. These groups can be combinate with each other in the secondary reaction, and be detected experimentally. For example, the decomposition products of PSA-Phen resin are dominated by benzene, toluene, naphthalene, and 2-methylnaphthalene, while the decomposition products of PSNP resin are mainly composed of naphthalene, 2-methylnaphthalene, and anthracene, which is caused by the difference of their backbone. Benzene and methylbenzene, two of the main products of the PSA-Phen detected, are the two components that account for the most in Guo's experiment [11], which is another verification of our simulation results. In addition, the degradation products of PSNP resins are also verified in the present experiments (Section 6 of the Supporting Information). The naphthalene and 2-methylnaphthalene are the main products, and anthracene is also a detectable product in gas chromatography/mass spectrometry (GC/MS).

Table 3
The simulation $Y_{800\ °C}$ vs. the experimental $Y_{800\ °C}$ of PSA-Phen and PSNP resins.

Resins	Sim. $Y_{800\ °C}$ (%)	Exp. $Y_{800\ °C}$ (%)
PSA-Phen	89.95	90.3
PSNP	92.51	92.3

4. Conclusion

In the present work, the thermal decomposition mechanism of two representatives of PSA resins with naphthyl and phenyl groups on the backbone (i.e., PSNP and PSA-Phen) was explored by ReaxFF MD simulations. The effects of heating rates, temperatures, and crosslinking degrees on the degradation products of cured PSA-Phen and PSNP resins were analyzed. And the simulation results revealed that for these two resins, the initial decomposition dominates below 2000 K, the secondary decomposition plays a leading role in the range from 2000 K to 2400 K, and 2600 K is the boundary between the secondary and final decomposition. This information is an important reference for the experimentalists. Kinetic analysis was applied to the resin degradation process, and the activation energy of the decomposition of the PSA-Phen resin calculated by simulation is close to the experimental value. Moreover, the predicted TGA curves of the resins are also consistent with the experimental results. The results theoretically verified that the PSNP resin has better heat resistance, which is mainly due to the fact that T_{d5} is dominated by the secondary decomposition and final decomposition. In this process, the higher molecular weight and the more stable C—C in the naphthyl lead to the higher thermal stability of PSNP resins. The overall thermal decomposition mechanism observed in simulations reveals the formation of intermediate and primary structures, such as benzene, methylbenzene, naphthalene, and methylnaphthalene. The simulation results can be the theoretical explanation of the experimental observations and strongly support the design of heat-resistant resins in the future.

CRediT authorship contribution statement

Yaxi Hu: Methodology, Software, Formal analysis, Data curation, Writing – original draft, Visualization. **Liquan Wang:** Investigation, Validation, Writing – review & editing, Project administration, Funding acquisition. **Liang Gao:** Writing – review & editing. **Jiaping Lin:** Conceptualization, Validation, Resources, Writing – review & editing, Supervision, Funding acquisition. **Lei Du:** Supervision.

Declaration of Competing Interest

The authors declare that they have no known competing financial interests or personal relationships that could have appeared to influence the work reported in this paper.

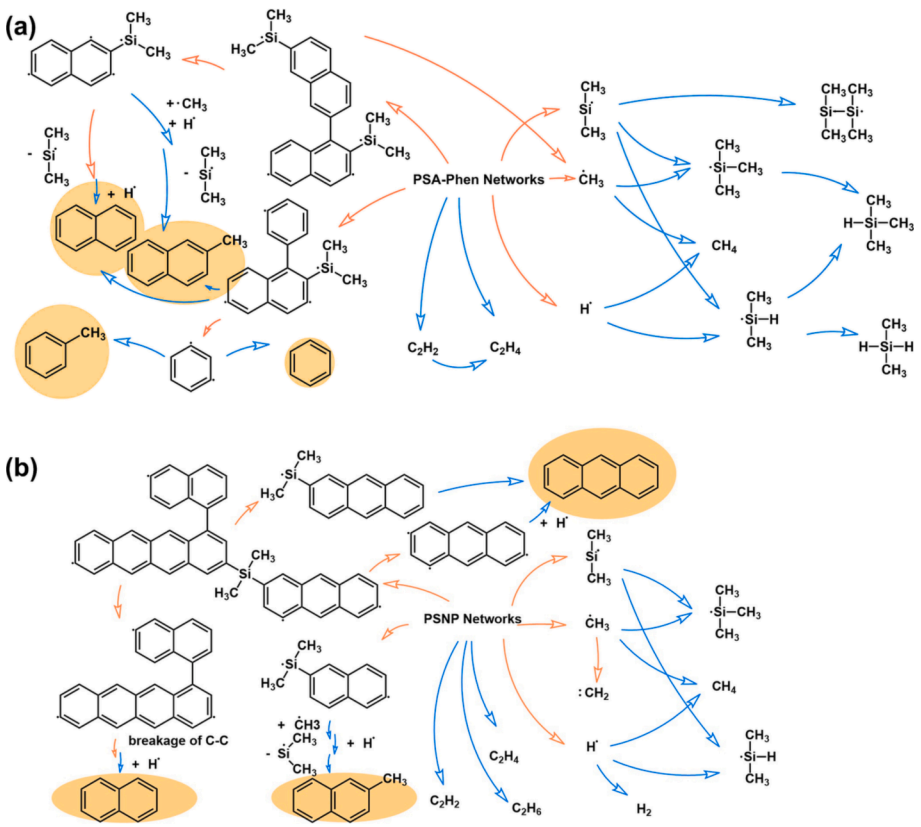

Fig. 10. Decomposition mechanism and main products of (a) PSA-Phen and (b) PSNP resins. The orange arrows represent the initial decomposition process, while the blue ones represent the secondary decomposition. Products verified by the experimental observations are marked with orange areas. The experimental observations corresponding to the PSA-Phen resins are from Ref 10, while the experimental observations corresponding to the PSNP resins are from the experiments of our present work (Section 6 of the Supporting information). (For interpretation of the references to colour in this figure legend, the reader is referred to the web version of this article.)

Data availability

Data will be made available on request.

Acknowledgments

This work was supported by the National Natural Science Foundation of China (51833003, 22173030, and 21975073).

Appendix A. Supplementary material

Supplementary data to this article can be found online at https://doi.org/10.1016/j.commatsci.2023.112502.

References

[1] M. Itoh, K. Inoue, N. Hirayama, M. Sugimoto, T. Seguchi, Fiber reinforced composites with a new heat-resistant polymer matrix containing silicon, J. Jpn. Soc. Compos. Mater. 27 (2001) 188–193, https://doi.org/10.6089/jscm.27.188.
[2] M. Ichitani, K. Nakamura, Cured product of carborane-containing silicon-base resin, Japanese Patent JP 2000309635, Japan (2000).
[3] K. Inoue, K. Iwata, J. Ishikawa, S. Fujikake, M. Itoh, Silicon-containing polymers for manufacture of ceramic moldings, Japanese Patent JP 19970428, Japan (2003).
[4] M. Itoh, M. Mitsuzuka, K. Iwata, K. Inoue, A novel synthesis and extremely high thermal stability of poly[(phenylsilylene)-ethynylene-1,3-phenyleneethynylene], Macromolecules 27 (1994) 7917–7919, https://doi.org/10.1021/ma00104a056.
[5] M. Itoh, K. Inoue, K. Iwata, J. Ishikawa, Y. Takenaka, A heat-resistant silicon-based polymer, Adv. Mater. 9 (1997) 1187–1190, https://doi.org/10.1002/adma.19970091514.
[6] J. Huang, W. Du, J. Zhang, F. Huang, L. Du, Study on the copolymers of silicon-containing arylacetylene resin and acetylene-functional benzoxazine, Polym. Bull. 62 (2009) 127–138, https://doi.org/10.1007/s00289-008-0003-1.
[7] J. Zhang, J. Huang, W. Du, F. Huang, L. Du, Thermal stability of the copolymers of silicon-containing arylacetylene resin and acetylene-functional benzoxazine, Polym. Degrad. Stab. 96 (2011) 2276–2283, https://doi.org/10.1016/j.polymdegradstab.2011.04.022.
[8] J. Zhu, M. Chu, Z. Chen, L. Wang, J. Lin, L. Du, Rational design of heat-resistant polymers with low curing energies by a materials genome approach, Chem. Mater. 32 (2020) 4527–4535, https://doi.org/10.1021/acs.chemmater.0c00238.
[9] S. Du, S. Zhang, L. Wang, J. Lin, L. Du, Polymer genome approach: a new method for research and development of polymers, Acta Polym. Sin. 53 (2022) 592–607, https://doi.org/10.11777/j.issn1000-3304.2021.21404.
[10] J. Zhang, J. Huang, W. Zhou, F. Huang, L. Du, Fiber reinforced silicon-containing arylacetylene resin composites, Express Polym. Lett. 1 (2007) 831–836, https://doi.org/10.3144/expresspolymlett.2007.115.
[11] K. Guo, P. Li, Y. Zhu, F. Wang, H. Qi, Thermal curing and degradation behaviour of silicon-containing arylacetylene resins, Polym. Degrad. Stab. 131 (2016) 98–105, https://doi.org/10.1016/j.polymdegradstab.2016.07.006.
[12] J.L. de La Fuente, M. Ruiz-Bermejo, C. Menor-Salván, S. Osuna-Esteban, Thermal characterization of HCN polymers by TG-MS, TG, DTA and DSC methods, Polym. Degrad. Stab. 96 (2011) 943–948, https://doi.org/10.1016/j.polymdegradstab.2011.01.033.
[13] B. Rotavera, C.A. Taatjes, Influence of functional groups on low-temperature combustion chemistry of biofuels, Prog. Energy Combust. Sci. 86 (2021), 100925, https://doi.org/10.1016/j.pecs.2021.100925.
[14] G. Dai, G. Wang, K. Wang, Z. Zhou, S. Wang, Mechanism study of hemicellulose pyrolysis by combining in-situ DRIFT, TGA-PIMS and theoretical calculation, Proc. Combust. Inst. 38 (2021) 4241–4249, https://doi.org/10.1016/j.proci.2020.06.196.
[15] J.A. Miller, M.J. Pilling, J. Troe, Unravelling combustion mechanisms through a quantitative understanding of elementary reactions, Proc. Combust. Inst. 30 (2005) 43–88, https://doi.org/10.1016/j.proci.2004.08.281.
[16] A.C.T. van Duin, S. Dasgupta, F. Lorant, W.A. Goddard, ReaxFF: A reactive force field for hydrocarbons, J. Phys. Chem. A 105 (2001) 9396–9409, https://doi.org/10.1021/jp004368u.
[17] D. Hong, L. Liu, C. Wang, T. Si, X. Guo, Construction of a coal char model and its combustion and gasification characteristics: Molecular dynamic simulations based on ReaxFF, Fuel 300 (2021), 120972, https://doi.org/10.1016/j.fuel.2021.120972.
[18] J.R. Gissinger, S.R. Zavada, J.G. Smith, J. Kemppainen, I. Gallegos, G.M. Odegard, et al., Predicting char yield of high-temperature resins, Carbon 202 (2023) 336–347, https://doi.org/10.1016/j.carbon.2022.11.002.
[19] A.M. Christmann, A.R. Muniz, Analysis of the effect of temperature and density on polyetherimide pyrolysis toward carbon molecular sieve membrane formation, Carbon 205 (2023) 97–111, https://doi.org/10.1016/j.carbon.2023.01.016.
[20] S. AlAreeqi, D. Bahamon, K. Polychronopoulou, L.F. Vega, Insights into the thermal stability and conversion of carbon-based materials by using ReaxFF reactive force field: Recent advances and future directions, Carbon 196 (2022) 840–866, https://doi.org/10.1016/j.carbon.2022.05.035.
[21] T.P. Senftle, S. Hong, M.M. Islam, S.B. Kylasa, Y. Zheng, Y.K. Shin, et al., The ReaxFF reactive force-field: Development, applications and future directions, npj Comput Mater. 2 (2016) 1–14, https://doi.org/10.1038/npjcompumats.2015.11.

[22] X. Li, M. Zheng, C. Ren, L. Guo, ReaxFF molecular dynamics simulations of thermal reactivity of various fuels in pyrolysis and combustion, Energy & Fuels 35 (2021) 11707–11739, https://doi.org/10.1021/acs.energyfuels.1c01266.
[23] X. Lu, X. Wang, Q. Li, X. Huang, S. Han, G. Wang, A ReaxFF-based molecular dynamics study of the pyrolysis mechanism of polyimide, Polym. Degrad. Stab. 114 (2015) 72–80, https://doi.org/10.1016/j.polymdegradstab.2015.02.004.
[24] Y. Zhong, X. Jing, S. Wang, Q.X. Jia, Behavior investigation of phenolic hydroxyl groups during the pyrolysis of cured phenolic resin via molecular dynamics simulation, Polym. Degrad. Stab. 125 (2016) 97–104, https://doi.org/10.1016/j.polymdegradstab.2015.11.017.
[25] M. Kowalik, C. Ashraf, B. Damirchi, D. Akbarian, S. Rajabpour, A.C.T. van Duin, Atomistic scale analysis of the carbonization process for C/H/O/N-based polymers with the ReaxFF reactive force field, J. Phys. Chem. B 123 (2019) 5357–5367, https://doi.org/10.1021/acs.jpcb.9b04298.
[26] Q. Mao, S. Rajabpour, M. Kowalik, A.C.T. van Duin, Predicting cost-effective carbon fiber precursors: Unraveling the functionalities of oxygen and nitrogen-containing groups during carbonization from ReaxFF simulations, Carbon 159 (2020) 25–36, https://doi.org/10.1016/j.carbon.2019.12.008.
[27] S. Zhang, S. Du, L. Wang, J. Lin, L. Du, X. Xu, et al., Design of silicon-containing arylacetylene resins aided by machine learning enhanced materials genome approach, Chem. Eng. J. 448 (2022), 137643, https://doi.org/10.1016/j.cej.2022.137643.
[28] M. Ma, N. Dai, X. Liu, C. Li, Q. Yuan, F. Huang, Reinforcing the poly(silylene arylacetylene)s via strong π-π stacking interactions, Polymer 229 (2021), 123976, https://doi.org/10.1016/j.polymer.2021.123976.
[29] F. Zheng, K. Wan, F. Huang, B. Niu, Y. Shi, D. Wei, et al., Assessing pyrolysis behavior of silicon-containing arylacetylene resin via experiments and ReaxFF MD simulations, J. Anal. Appl. Pyrolysis 164 (2022), 105528, https://doi.org/10.1016/j.jaap.2022.105528.
[30] Z. Ling, J. Zhu, C. Cai, J. Lin, L. Wang, L. Du, Highly heat-resistant branched silicon-containing arylacetylene resins with low curing temperature, Polym. Int. 70 (2021) 1595–1603, https://doi.org/10.1002/pi.6254.
[31] G. Gao, S. Zhang, L. Wang, J. Lin, H. Qi, J. Zhu, et al., Developing highly tough, heat-resistant blend thermosets based on silicon-containing arylacetylene: a material genome approach, ACS Appl. Mater. Inter. 12 (2020) 27587–27597, https://doi.org/10.1021/acsami.0c06292.
[32] S. Gandon, P. Mison, M. Bartholin, R. Mercier, B. Sillion, E. Geneve, et al., Thermal polymerization of arylacetylenes: 1. Study of a monofunctional model compound, Polymer 38 (1997) 1439–1447, https://doi.org/10.1016/S0032-3861(96)00658-1.
[33] S. Gandon, P. Mison, B. Sillion, Thermal polymerization of arylacetylenes: 2. Study of linear dimers, Polymer 38 (1997) 1449–1459, https://doi.org/10.1016/S0032-3861(97)89718-2.
[34] X. You, S. Deng, Y. Huang, Z. Liu, Y. Hu, Thermosetting mechanism study of silicon-containing polyarylacetylene via in situ FTIR and solid-state NMR spectroscopy, J. Appl. Polym. Sci. 136 (2019) 47301, https://doi.org/10.1002/app.47301.
[35] L. Lu, K. Guo, J. Zhu, F. Wang, Y. Zhu, H. Qi, Silicon-containing fluorenylacetylene resins with low curing temperature and high thermal stability, J. Appl. Polym. Sci. 136 (2019) 48262, https://doi.org/10.1002/app.48262.
[36] BIOVIA Materials Studio. https://www.3ds.com/products-services/biovia/products/molecular-modeling-simulation/biovia-materials-studio/ (accessed 2023-05-08).
[37] S. Plimpton, Fast parallel algorithms for short-range molecular dynamics, J. Comput. Phys. 117 (1995) 1–19, https://doi.org/10.1006/jcph.1995.1039.
[38] A.D. Kulkarni, D.G. Truhlar, S. Goverapet Srinivasan, A.C.T. van Duin, P. Norman, T.E. Schwartzentruber, Oxygen interactions with silica surfaces: Coupled cluster and density functional investigation and the development of a new ReaxFF potential, J. Phys. Chem. C 117 (2013) 258–269, https://doi.org/10.1021/jp3086649.
[39] K. Chenoweth, A.C.T. van Duin, W.A. Goddard, ReaxFF reactive force field for molecular dynamics simulations of hydrocarbon oxidation, J. Phys. Chem. A 112 (2008) 1040–1053, https://doi.org/10.1021/jp709896w.
[40] D. Hong, Z. Cao, X. Guo, Effect of calcium on the secondary reactions of tar from Zhundong coal pyrolysis: A molecular dynamics simulation using ReaxFF, J. Anal. Appl. Pyrol. 137 (2019) 246–252, https://doi.org/10.1016/j.jaap.2018.11.033.
[41] H.J.C. Berendsen, J.P.M. Postma, W.F. van Gunsteren, A. Dinola, J.R. Haak, Molecular dynamics with coupling to an external bath, J. Chem. Phys. 81 (1984) 3684–3690, https://doi.org/10.1063/1.448118.
[42] T. Zhang, X. Li, X. Qiao, M. Zheng, L. Guo, W. Song, et al., Initial mechanisms for an overall behavior of lignin pyrolysis through large-scale ReaxFF molecular dynamics simulations, Energy & Fuels 30 (2016) 3140–3150, https://doi.org/10.1021/acs.energyfuels.6b00247.
[43] T. Dyakonov, P.J. Mann, Y. Chen, W.T.K. Stevenson, Thermal analysis of some aromatic amine cured model epoxy resin systems - II: Residues of degradation, Polym. Degrad. Stab. 54 (1996) 67–83, https://doi.org/10.1016/0141-3910(96)00096-1.
[44] Y. Wang, S. Wang, C. Bian, Y. Zhong, X. Jing, Effect of chemical structure and crosslink density on the heat resistance of phenolic resin, Polym. Degrad. Stab. 111 (2015) 239–246, https://doi.org/10.1016/j.polymdegradstab.2014.11.016.
[45] A. Lele, H. Kwon, K. Ganeshan, Y. Xuan, A.C.T. van Duin, ReaxFF molecular dynamics study on pyrolysis of bicyclic compounds for aviation fuel, Fuel 297 (2021), 120724, https://doi.org/10.1016/j.fuel.2021.120724.
[46] R.F.B. Goncalves, B.K.V. Iha, J.A.F.F. Rocco, A.E. Kuznetsov, Reactive molecular dynamics of pyrolysis and combustion of alternative jet fuels: A ReaxFF study, Fuel 310 (2022), 122157, https://doi.org/10.1016/j.fuel.2021.122157.
[47] M. Xu, S. Shi, Y. Wang, L. Zhang, Thermal pyrolytic behaviors and kinetics of silicon-containing arylacetylene resin, Fiber Reinf Plast./Compos. 6 (2010) 35–39, https://doi.org/10.3969/j.issn.1003-0999.2010.06.009.
[48] M. Shanshal, M.M. Muala, C-C bond cleavage in aromatic molecules; benzene, toluene and naphthalene, Jordan J. Chem. 8 (2013) 113–124, https://doi.org/10.12816/0001522.